Erschienen in: Advanced Materials ; 30 (2018), 1. - 1703612
https://dx.doi.org/10.1002/adma.201703612

Nanomorphology Effects in Semiconductors with Native Ferromagnetism: Hierarchical Europium (II) Oxide Tubes Prepared via a Topotactic Nanostructure Transition

*Bastian Trepka, Philipp Erler, Severin Selzer, Tom Kollek, Klaus Boldt, Mikhail Fonin, Ulrich Nowak, Daniel Wolf, Axel Lubk, and Sebastian Polarz**

Semiconductors with native ferromagnetism barely exist and defined nanostructures are almost unknown. This lack impedes the exploration of a new class of materials characterized by a direct combination of effects on the electronic system caused by quantum confinement effects with magnetism. A good example is EuO for which currently no reliable routes for nanoparticle synthesis can be established. Bottom-up approaches applicable to other oxides fail because of the labile oxidation state +II. Instead of targeting a direct synthesis, the two steps—"structure control" and "chemical transformation"—are separated. The generation of a transitional, hybrid nanophase is followed by its conversion into EuO under full conservation of all morphological features. Hierarchical EuO materials are now accessible in the shape of oriented nanodisks stacked to tubular particles. Magnetically, the coupling of either vortex or onion states has been found. An unexpected temperature dependence is governed by thermally activated transitions between these states.

The enormous technological importance of semiconductors on the one hand and ferromagnetic materials on the other is beyond dispute. A new set of properties and applications in spintronics is expected for a direct combination of magnetism with semiconductor properties.[1] Considering the well-known quantum-size effect for semiconductors, it would be interesting to study a magnetic material with its electronic properties changing with size, as pointed out by Stoll and co-workers.[2,3] Significant progress has been made for diluted magnetic semiconductor compounds such as GaN doped with paramagnetic ions such as Mn(II).[4] However, there are limited examples for solids with native ("undiluted") semiconductor ferromagnetism. Only little attention was devoted to semiconductor ferromagnets such as GdN, SmN, EuO, or EuS in the past.[5–7] When it comes to bulk materials, Europium(II) oxide is the most studied. The band gap of EuO (E_{gap} = 1.1 eV) is similar to silicon and it can be described as an almost ideal Heisenberg ferromagnet with a high magnetic moment of 7 μ_B per Eu^{2+}.[8,9] Key features in the electronic structure originate from localized Eu 7 4f-states in the gap causing large Zeeman splitting of the conduction band below the Curie temperature T_C = 69 K.[10] EuO is a half metal with the spin polarization approaching 100%,[8,9] making it an ideal candidate for spintronic applications such as spin filtering.[11]

Despite the exceptional properties of EuO almost nothing is known when it comes to nanomaterials, except for thin films prepared by ultrahigh vacuum deposition methods.[12] The difficulties in preparing nanostructured EuO are caused by the required high temperatures (1200 K) and the need for a very precise control of stoichiometry.[13] Low-temperature, soft-chemistry methods such as sol–gel processing fail because of the reducing character of Eu^{2+} ($U_{EuII/EuIII}$ = −0.35 V), which is sufficient to react with water resulting in Eu_2O_3 as the preferred species.[14,15] However, the work of Yanagida and co-workers needs to be mentioned, who could prepare EuO nanoparticles with sizes below 10 nm by the photoreduction of $Eu(NO_3)_3$,[16] and before that by means of the reaction of Eu metal in liquid ammonia.[17]

In our current contribution, we introduce a different strategy. We first prepare a defined nanostructure of an Eu-containing material, which is subsequently transformed to EuO under full preservation of all the features of this nanostructure. Similarities can be seen to metal oxide materials generated from converting metal–organic framework materials as a precursor phase.[18,19] In particular, we aim at a material consisting of stacked EuO sheets with a central hole because these may show a special feature of magnetism, namely magnetic vortex states with alternating chirality. Chiral magnetic textures, e.g., skyrmions,[20,21] have been in the focus of modern magnetism because of their potential for applications in data storage and spintronics.

B. Trepka, T. Kollek, Dr. K. Boldt, Prof. S. Polarz
Department of Chemistry
University of Konstanz
Universitaetsstrasse 10, D-78457 Konstanz, Germany
E-mail: sebastian.polarz@uni-konstanz.de
Dr. P. Erler, S. Selzer, Prof. M. Fonin, Prof. U. Nowak
Department of Physics
University of Konstanz
Universitaetsstrasse 10, D-78457 Konstanz, Germany
Dr. D. Wolf, Dr. A. Lubk
IFW Dresden e.V.
Helmholtzstraße 20, D-01069 Dresden, Germany

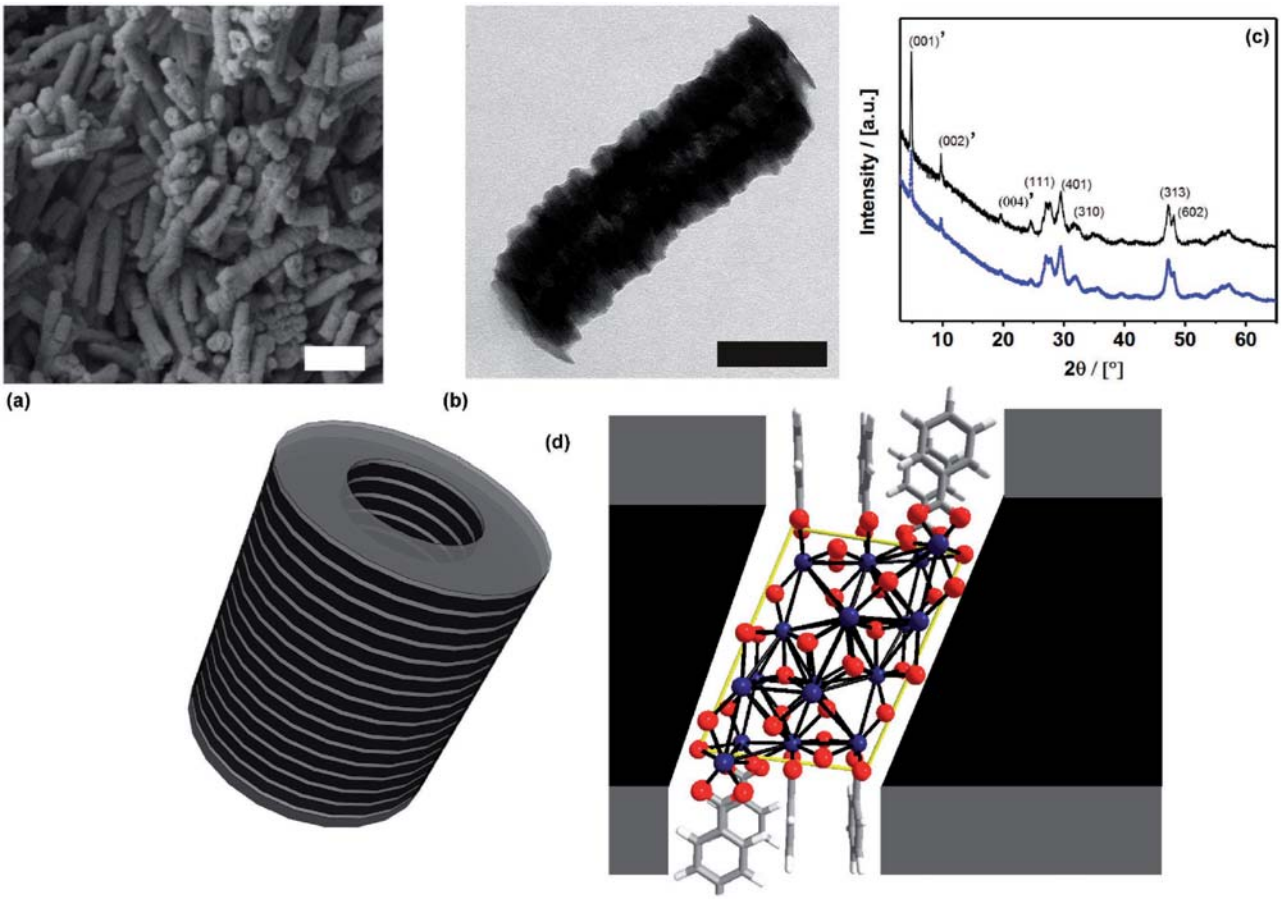

Figure 1. Structure of the hollow Eu(III)-benzoate nanotubes. a) SEM image; scale bar = 400 nm. b) TEM image; scale bar = 100 nm. A magnified image is given in Figure S2 in the Supporting Information. c) PXRD data. (') indicates signals corresponding to the lamellar substructure. Black curve = experiment pattern obtained from the hybrid material. Blue curve = simulated pattern with the structure model presented in (d). Blue = Eu; red = oxygen; dark gray = carbon; light gray = hydrogen; yellow = cell edges of monoclinic Eu_2O_3.

In a classical sol–gel process a suitable precursor is hydrolyzed and the oxide forms during polycondensation. This method is obviously not applicable here because water would oxidize Eu(II). Thus, in our synthesis strategy we wanted to perform nonaqueous sol–gel chemistry with a special Eu(II) naphtholate precursor (see also Figure S1, Supporting Information).[22] Niederberger showed in his pioneering work that the conversion with benzyl alcohol under solvothermal conditions represents a versatile method for the synthesis of diverse metal oxide nanomaterials.[23] We adopted similar conditions, receiving a material with intriguing structure shown in **Figure 1**. Scanning electron microscopy (SEM) images show cylinders with extension in the μm range. The diameter (≈120 nm) is remarkably uniform, and there seems to be an opening at the end of the particles. The hollow character can be confirmed by transmission electron microscopy (TEM) images shown in Figure 1b, in which the middle section of the particle appears lighter. Occasionally, particles (or fragments) lay perpendicular to the long-axis on the TEM grid (see Figure S2, Supporting Information), which confirms the presence of a cavity with a diameter of 30–50 nm. The tubes have a lamellar substructure (Figure 1b) with a periodicity of 1.8 nm. Because there is pronounced imaging contrast, one may already guess the two phases are characterized by a substantial difference in electron density of the involved atoms.

Further evidence for the structure of the materials comes from powder X-ray diffraction (PXRD) shown in Figure 1c. The noted pattern agrees nicely with layers of slightly distorted, monoclinic Eu_2O_3 separated by an organic phase. This is consistent with the quantitative transformation of Eu(II) from the precursor to Eu(III) (confirmed by superconducting quantum interference device (SQUID) measurements shown in Figure S2, Supporting Information). We conclude the material consists of monoclinic Eu_2O_3 sheets grown in *b* and *c* direction with a thickness of one lattice parameter in *a*-direction because the width of the dark stripes seen in TEM (1.3 nm) is uniform and fits very well with the lattice parameter $a = 1.41$ nm (Figure 1d). Growth in *a*-direction is prohibited by organic cappers bound to the (100) and (–100) atomic planes. For determining the nature of those capping agents, the material was dissolved and analyzed by electron spray ionization mass spectrometry (ESI-MS), Fourier transform (FT-IR) spectroscopy, and thermogravimetric analysis (TGA) (data shown in Figure S2, Supporting Information). The observed ESI-MS pattern agrees well with the benzoate species present in the hybrid material. According to TGA there are 0.7 benzoate units per Eu atom. As the monoclinic Eu_2O_3 cell contains 12 Eu atoms we

expect eight benzoate cappers in total, four attached to the (100) facet and four at the opposite (–100) surface (see Figure 1d).

Crucial questions are not only how the described hybrid phase forms but also what the origin of the cavity is. We have examined samples taken at different times during the early stages of the solvothermal reaction by TEM. The described series is shown in Figure S3 in the Supporting Information. Nanorods with a diameter of ≈30 nm form very early in the reaction mixture (t = 5 min). At lower temperature, we were able to grow single crystals of this initial phase, and the structure was resolved by X-ray diffraction techniques (Figure S4, Supporting Information). A new molecular compound formed comprising a core of eight Eu-centers in a cube-like arrangement held together by Eu-O-Eu bridges. Both naphtholate and benzyl alcohol coordinate to Eu. From studies on the benzyl alcohol process applied to Y, Nd, Gd, or Sm[24,25] it is known that the metal centers catalyze a hydride transfer reaction from benzyl alcohol ligands to form a hydroxyl group at the metal, and benzaldehyde and toluene are released. The former can condensate with another metal under release of a ligand. Over time (t > 13 min) benzaldehyde is transformed to benzoate and toluene in a second step via a Canizzaro-like reaction (see Figure S5, Supporting Information). As a result, the nanorods formed under solvothermal conditions represent nucleation sites for the assembly of the Eu_2O_3-benzoate hybrid at the lateral surfaces (Figure S3, Supporting Information). Finally, at t = 40 min, the inner core comprising the intermediate phase is consumed, leaving the final, hollow particles behind (t = 160 min). The formation mechanism of the hybrid tubes is summarized in Figure S3 in the Supporting Information. Reaction temperature studies were performed in a range from 180 to 250 °C (see Figure S6, Supporting Information). At any given temperature, the hybrid tubes are formed, demonstrating the high reproducibility and reliability of the synthesis protocol. With increasing reaction temperature, the length of the nanotubes increases. Alternative morphologies such as spherical particles can be realized by starting from $Eu(II)(OCH_2CH_2OCH_3)_2$,[26] which proves the high relevance of the chemical nature of the precursor (see Figure S7, Supporting Information) indicating that the $Eu(ONpht)_2$ precursor is essential for the generation of the nanotubes reported here.

One way to produce EuO is the reaction of Eu_2O_3 with a vapor of elemental Eu.[15] Due to the lamellar hybrid nanostructure described above, we expect maximal accessibility of Eu vapor to the Eu_2O_3 layers (**Figure 2**a). The specific surface area of the hybrid material determined from gas-physisorption measurements (Figure S2, Supporting Information) is remarkably high (90 $m^2\ g^{-1}$). Also, the inner cavity will facilitate a possible reaction. PXRD measurements shown in Figure 2b prove the resounding success of the proposed method. A phase pure material containing only Eu(II)O could be obtained. The lattice spacing (2.97 Å) determined using high resolution TEM (HRTEM) (Figure 2e) fits nicely to the (111) atomic plane distance (2.9698 Å) in single-crystalline EuO with rock salt structure (Fm-3m). From electron microscopy data (Figure 2c–e; for SEM see Figure S8, Supporting Information) one can deduce complete conservation of the nanostructure encoded at the previous stage as indicated in Figure 2a. The EuO particles do not only preserve rod-like shape, also the tubular character and lamellar structure is still present. The hollow characteristics of the nanostructure could be confirmed by SEM, TEM tomography analysis (Figure 2f), and line-scan energy-dispersive X-ray spectroscopy scans (see Figure S8, Supporting Information).

A reaction, for which one finds distinct (crystallographic) orientational relationships between starting material and product, is called topotactic, which is why we use the term topotactic nanostructure transition for the case described here. The occurrence of spots rather than diffraction rings in electron diffraction (ED) from single, isolated particles (Figure 2d) confirms the presence of rock salt-EuO as well as highly defined crystal orientation in each of the layers. Considering the temperature for the reduction to EuO is 500 °C, such a pronounced preservation of structural information is remarkable. Thus, we could fabricate a unique EuO nanostructure, which is only accessible via the special route described by us, and by no means in a direct manner.

The special nanostructure leads to important changes and improvement in key magnetic properties, probed by SQUID magnetometry. The data for the hierarchical EuO nanotubes (noted as EuO-1) are compared to two samples as references (**Figure 3**a). One sample consists of EuO nanotubes, but without the lamellar substructure (EuO-2); all relevant information is summarized in Figures S9 and S10 in the Supporting Information. Second, we have prepared nonstructured EuO (EuO-3) from a commercial Eu_2O_3 powder (see Figure S11, Supporting Information). Field-dependent measurements are given in Figure 3a,b. The coercivity of EuO-1 is much higher than for the reference samples and raised by a factor of ≈10 compared to values presented in the literature.[15] However, several additional features are unusual: EuO-2,3 behave as expected in T-dependent measurements with a ferromagnetic phase transition at 69 K and saturation below, which is in good agreement with the Curie temperature (T_c) reported in literature. EuO-1 is different. Magnetic polarization is not directly saturated after reaching T_c, and at T = 18.5 K there is even an increase in magnetization, which can be seen nicely from the maximum in the zero field cooled (ZFC) curve. Magnetization then drops at even lower temperatures indicating an antiferromagnetic contribution. Closer inspection (Figure 3b) reveals there is a second opening of the magnetization curves at higher field. A so-called butterfly hysteresis is characteristic for magnetic vortex states,[27] which could explain the marked differences in magnetic behavior compared to bulk EuO.

To support our conclusion we performed micromagnetic simulations based on the graphics processing unit (gpu)-accelerated open-source program MuMax^3 (for the material parameters and further technical information see simulations section, Supporting Information).[28] We simulate lamellar, elongated EuO-nanotubes constructed from an array of 33 rings with an outer diameter of 80 nm, an inner diameter of 20 nm, and a thickness of 4 nm. The layers are separated from each other by nonmagnetic layers of the same size. As a result, the interlayer coupling rests only on dipole–dipole interactions (stray field energy). Furthermore, we also simulate single, isolated rings for comparison. The ground state of the single ring is a flux-closure magnetic state, a vortex state, as it can be expected for thin film magnetic elements with sizes above the exchange length.[27] For EuO this is less than 3 nm. In the nanotubes, these states still interact. In order to minimize the stray field energy an ordered structure of antiferromagnetically

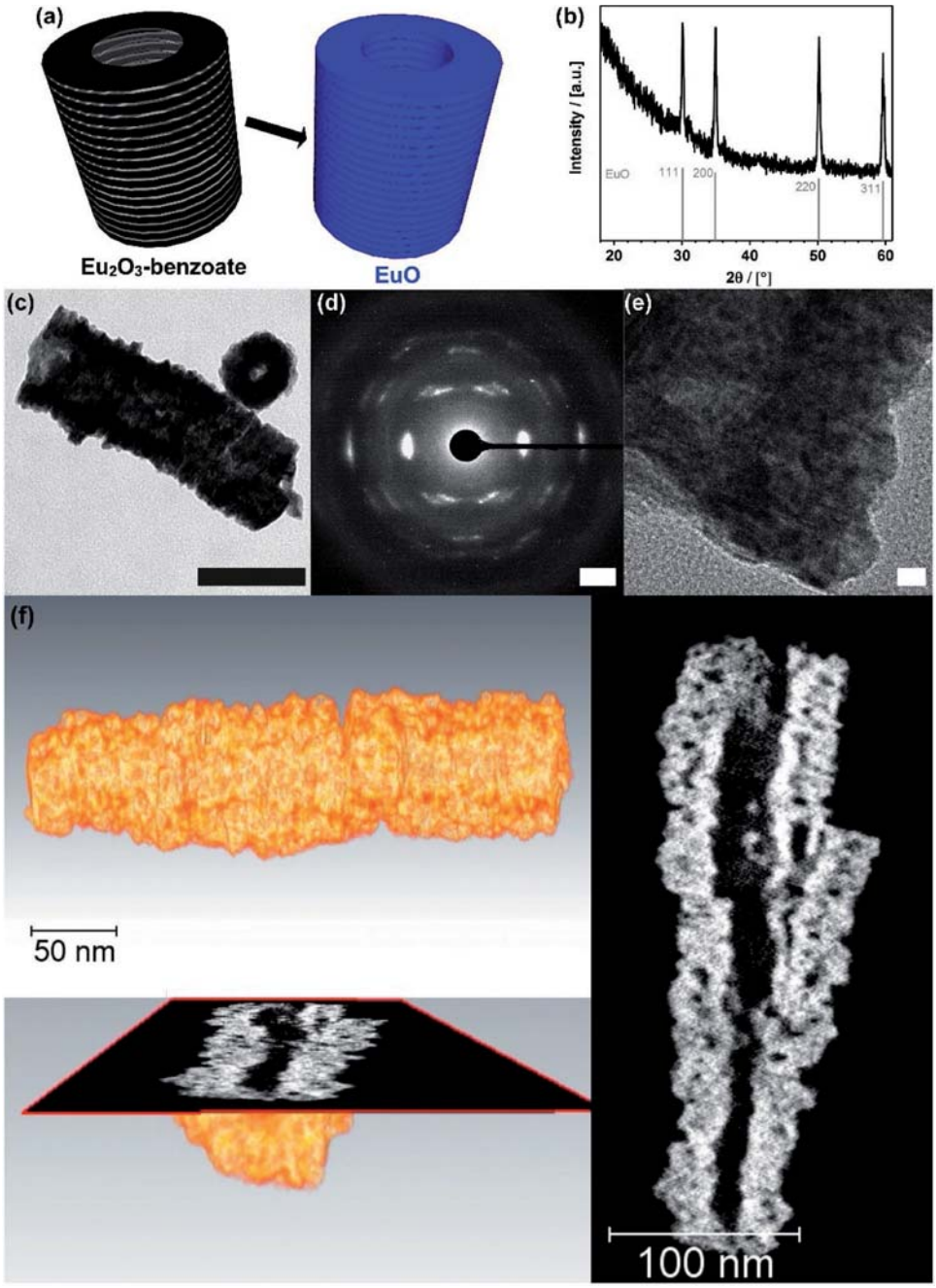

Figure 2. a) Transition from the hybrid phase (black/gray) to hierarchical EuO nanotubes (blue). PXRD (b), TEM (c, scale bar = 100 nm); ED (d, scale bar = 0.2 $Å^{-1}$); HRTEM (e, scale bar = 5 nm) of the EuO nanotubes. f) Images from TEM tomography series (movies are given in the Supporting Information).

coupled vortices arises (see left configuration of **Figure 4**b and the cut out in Figure 4c). This negative coupling was already discussed in Ref. [27] for magnetic bilayers.

For simulations with applied magnetic field we simulate the two extreme cases with the external field either along the long axis of the nanotube or perpendicular to it. For longitudinal direction, we see a butterfly hysteresis curve where the second opening at higher fields results from vortex nucleation and annihilation (Figure 4a). For perpendicular orientation, the remanent state of the single ring is a so-called onion state with its magnetization in field direction and two vortex walls (Figure 4e). In the past, onion states in magnetic ring structures have been used to control magnetic domains wall positions via external fields.[29] Since the onions state can be seen as a dipole, with the two poles built by the two domain walls on opposite side of the ring, the domain walls follow the direction of the external field.

In the nanotube, however, the situation is different. Because of the dipolar coupling the remanent state is again

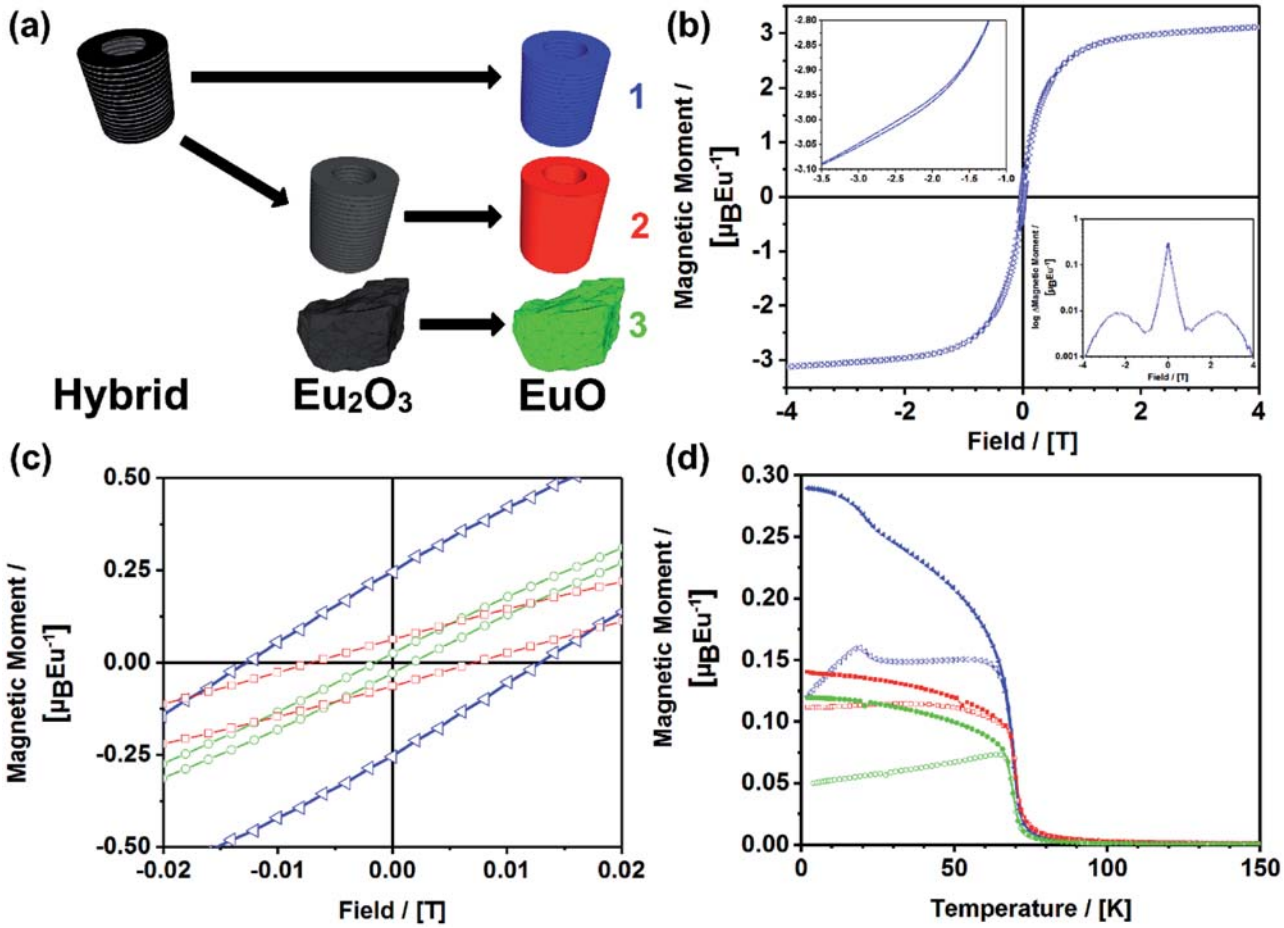

Figure 3. a) Overview of relevant samples. Hierarchical EuO nanotubes (blue) prepared from the hybrid material. EuO nanotubes (red) without the lamellar substructure prepared via Eu_2O_3 nanotubes as an interim stage (dark gray). EuO powder (green) prepared from a commercial Eu_2O_3 powder as a reference sample. b) Field-dependent magnetization curve ($T = 1.8$ K) for the hierarchical EuO nanotubes. The insets show a magnification of one sector of the magnetization curve and the deviation spectrum to illustrate the butterfly behavior. c) Comparison of the hysteresis area for the three EuO samples. d) *T*-dependent measurements with an applied magnetic field of 10 mT for the three EuO samples. Open symbols = zero field cooled (ZFC) measurements; solid symbols = field cooled (FC) measurements.

antiferromagnetically coupled with the magnetization of the onion states perpendicular to the field direction (center configuration of Figure 4b and corresponding cut out in Figure 4d). Microscopically, an antiferromagnetic spin configuration which is aligned mostly perpendicular to the applied field is known as spin flop phase. It arises in antiferromagnets when the field energy overcomes the local anisotropy.[30] Further, the onion state of the lamellar rings within the tube prefer mostly transverse walls. This wall type has higher stray field energy but this disadvantage is overcome by the antiferromagnetic coupling between adjacent rings which minimizes the stray-field energy.

With regard to our magnetic measurements, we note that in our samples we find distributed properties regarding the size and shape of the nanotubes as well as their orientation with respect to the external field. Also, in real samples pinning effects might play a role which can hardly be taken into account in our simulations. However, from our simulations we conclude that upon field cooling or coming from the saturated state during hysteresis the nanotubes are preferentially in the antiferromagnetically coupled onion state. After zero-field cooling the nanotubes adopt rather their magnetic ground state—the antiferromagnetically coupled vortex state. We suspect that upon heating thermally activated transitions from onion states with transverse domain walls to either vortex states or onion states with vortex wall occur. This might explain the decay of the magnetization around 18.5 K in Figure 3d.

The possibility to realize and to control intricate magnetic states in nanostructures made of magnetic semiconductors offers a great potential for the realization of novel spintronic devices fully compatible with the current semiconductor industry. Before, there were major obstacles in preparing defined nanostructures of the ferromagnetic semiconductor EuO because either traditional methods require too harsh reaction conditions or bottom-up techniques such as aqueous sol–gel methods fail considering the low stability of the oxidation state +II of Eu. These obstacles have now been overcome. We have presented a new route toward complex EuO nanomaterials. Instead of a direct synthesis, we could first generate hierarchical nanotubes of a layered monoclinic Eu_2O_3-organic hybrid, which was then converted quantitatively into EuO

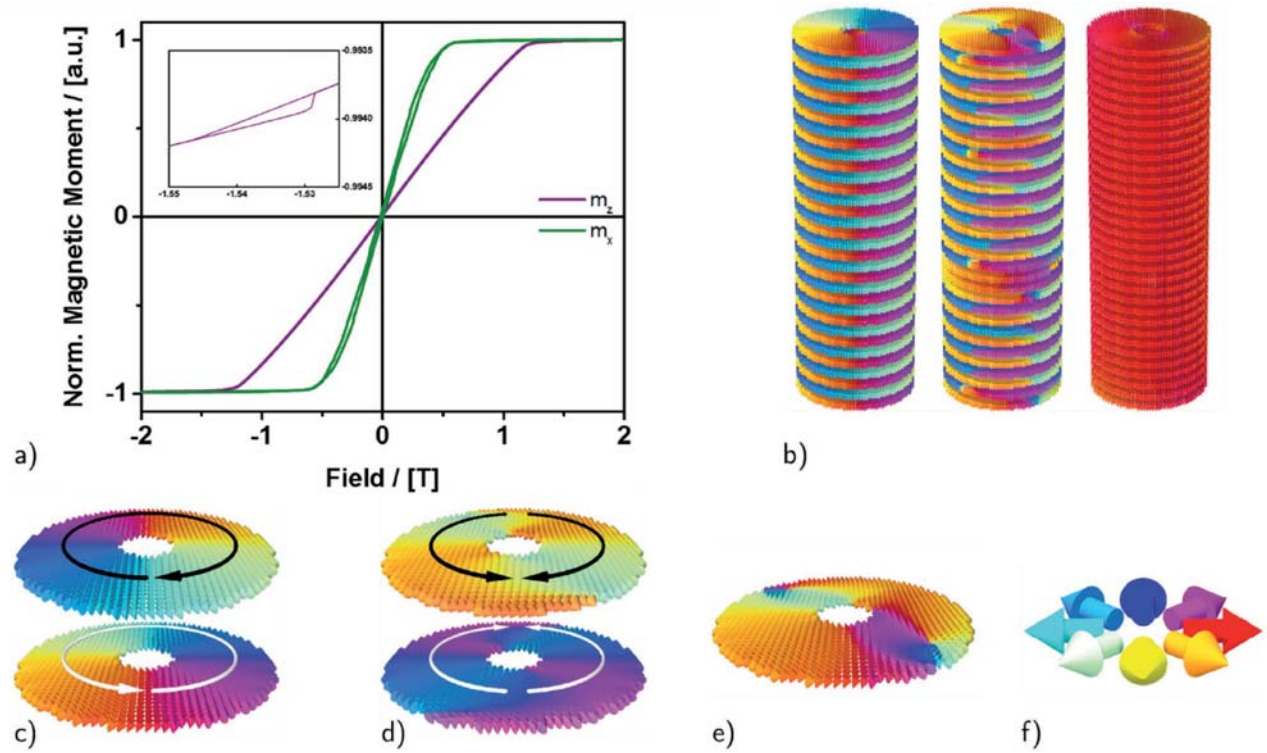

Figure 4. Simulation results: a) Calculated hysteresis curves for magnetic field direction parallel (*z*) and perpendicular (*x*) to the long axis of the tube; b) ground state, remanent state, and saturated magnetic state of the simulated nanotube (from left to right); c) two adjacent disks cut out from the ground state configuration showing antiferromagnetically coupled vortex states; d) two adjacent disks cut out from the remanent state showing antiferromagnetically coupled onion states; e) different version of an onion state with vortex walls; f) color coding.

under full preservation of all structural features. The resulting magnetic behavior was distinct from the bulk and shows the large impact of nanoparticle shape on magnetic properties. Size and shape influence strongly the properties of magnetic materials, and the soft-chemistry method presented here might open a route to access the according EuO nanoparticles via the generation of appropriate organic–inorganic hybrid nanoparticles first. It could already be shown that temperature and precursor characteristics influence particle length and morphology. However, much more research has to be invested for obtaining monodisperse sample and to obtain compact rather than hollow nanotubes.

Experimental Section

Methods and experimental details are given in the Supporting Information.

Supporting Information

Supporting Information is available from the Wiley Online Library or from the author.

Acknowledgements

The research was funded by the Deutsche Forschungsgemeinschaft DFG within the framework of the collaborative research center SFB-1214 (project A5). K.B. acknowledges support from the Fonds der Chemischen Industrie through a Liebig Fellowship. A.L. and D.W. acknowledge funding from the European Research Council via the ERC-2016-STG starting grant ATOM. A.L. and D.W. further express their gratitude to R. Hübner (Helmholtz Zentrum Dresden-Rossendorf) for helping with recording the tilt series.

Conflict of Interest

The authors declare no conflict of interest.

Keywords

hollow nanostructures, magnetic semiconductors, nonaqueous sol–gel process, shape–property relationships, vortex magnetism

[1] I. Zutic, J. Fabian, S. Das Sarma, *Rev. Mod. Phys.* **2004**, *76*, 323.
[2] W. Boncher, H. Dalafu, N. Rosa, S. Stoll, *Coord. Chem. Rev.* **2015**, *289–290*, 279.
[3] R. Beaulac, P. I. Archer, S. T. Ochsenbein, D. R. Gamelin, *Adv. Funct. Mater.* **2008**, *18*, 3873.
[4] T. Dietl, *Nat. Mater.* **2010**, *9*, 965.
[5] F. Natali, B. J. Ruck, H. J. Trodahl, D. Le Binh, S. Vezian, B. Damilano, Y. Cordier, F. Semond, C. Meyer, *Phys. Rev. B* **2013**, *87*, 035202.

[6] J. F. McNulty, B. J. Ruck, H. J. Trodahl, *Phys. Rev. B* **2016**, *93*, 054413.
[7] P. G. Steeneken, L. H. Tjeng, I. Elfimov, G. A. Sawatzky, G. Ghiringhelli, N. B. Brookes, D. J. Huang, *Phys. Rev. Lett.* **2002**, *88*, 047201.
[8] A. Schmehl, V. Vaithyanathan, A. Herrnberger, S. Thiel, C. Richter, M. Liberati, T. Heeg, M. Rockerath, L. F. Kourkoutis, S. Muhlbauer, P. Boni, D. A. Muller, Y. Barash, J. Schubert, Y. Idzerda, J. Mannhart, D. G. Schlom, *Nat. Mater.* **2007**, *6*, 882.
[9] H. X. Yang, A. Hallal, D. Terrade, X. Waintal, S. Roche, M. Chshiev, *Phys. Rev. Lett.* **2013**, *110*, 046603.
[10] B. T. Matthias, R. M. Bozorth, J. H. Van Vleck, *Phys. Rev. Lett.* **1961**, *7*, 160.
[11] C. Caspers, A. Gloskovskii, M. Gorgoi, C. Besson, M. Luysberg, K. Z. Rushchanskii, M. Lezaic, C. S. Fadley, W. Drube, M. Muller, *Sci. Rep.* **2016**, *6*, 22912.
[12] T. Mairoser, J. A. Mundy, A. Melville, D. Hodash, P. Cueva, R. Held, A. Glavic, J. Schubert, D. A. Muller, D. G. Schlom, A. Schmehl, *Nat. Commun.* **2015**, *6*, 8716.
[13] M. W. Shafer, *J. Appl. Phys.* **1965**, *36*, 1145.
[14] G. S. Wu, L. D. Zhang, B. C. Cheng, T. Xie, X. Y. Yuan, *J. Am. Chem. Soc.* **2004**, *126*, 5976.
[15] M. J. Bierman, K. M. Van Heuvelen, D. Schmeißer, T. C. Brunold, S. Jin, *Adv. Mater.* **2007**, *19*, 2677.
[16] Y. Hasegawa, S. Thongchant, Y. Wada, H. Tanaka, T. Kawai, T. Sakata, H. Mori, S. Yanagida, *Angew. Chem., Int. Ed.* **2002**, *41*, 2073.
[17] S. Thongchant, Y. Hasegawa, Y. Wada, S. Yanagida, *Chem. Lett.* **2001**, *30*, 1274.
[18] M. Y. Masoomi, A. Morsali, *Coord. Chem. Rev.* **2012**, *256*, 2921.
[19] T. K. Kim, K. J. Lee, J. Y. Cheon, J. H. Lee, S. H. Joo, H. R. Moon, *J. Am. Chem. Soc.* **2013**, *135*, 8940.
[20] T. Shinjo, T. Okuno, R. Hassdorf, K. Shigeto, T. Ono, *Science* **2000**, *289*, 930.
[21] M. Nagao, Y.-G. So, H. Yoshida, M. Isobe, T. Hara, K. Ishizuka, K. Kimoto, *Nat. Nanotechnol.* **2013**, *8*, 325.
[22] J. Carretas, J. Branco, J. Marcalo, P. Isolani, A. Domingos, A. de Matos, *J. Alloys Compd.* **2001**, *323*, 169.
[23] M. Niederberger, *Acc. Chem. Res.* **2007**, *40*, 793.
[24] N. Pinna, G. Garnweitner, P. Beato, M. Niederberger, M. Antonietti, *Small* **2005**, *1*, 112.
[25] M. Karmaoui, R. A. Sá Ferreira, A. T. Mane, L. D. Carlos, N. Pinna, *Chem. Mater.* **2006**, *18*, 4493.
[26] W. J. Evans, M. A. Greci, J. W. Ziller, *Inorg. Chem.* **1998**, *37*, 5221.
[27] K. Y. Guslienko, *J. Nanosci. Nanotechnol.* **2008**, *8*, 2745.
[28] A. Vansteenkiste, J. Leliaert, M. Dvornik, M. Helsen, F. Garcia-Sanchez, B. V. Waeyenberge, *AIP Adv.* **2014**, *4*, 107133.
[29] M. Klaui, C. A. F. Vaz, L. Lopez-Diaz, J. A. C. Bland, *J. Phys.: Condens. Matter* **2003**, *15*, R985.
[30] S. Chikazumi, *Physics of Ferromagnetism*, OUP, Oxford, **2009**.